



Since January 2020 Elsevier has created a COVID-19 resource centre with free information in English and Mandarin on the novel coronavirus COVID-19. The COVID-19 resource centre is hosted on Elsevier Connect, the company's public news and information website.

Elsevier hereby grants permission to make all its COVID-19-related research that is available on the COVID-19 resource centre - including this research content - immediately available in PubMed Central and other publicly funded repositories, such as the WHO COVID database with rights for unrestricted research re-use and analyses in any form or by any means with acknowledgement of the original source. These permissions are granted for free by Elsevier for as long as the COVID-19 resource centre remains active.



Mechanism of an RBM-targeted rabbit monoclonal antibody 9H1 neutralizing SARS-CoV-2



Xiaoyu Chu^{a,1}, Xinyu Ding^{b,c,1}, Yixuan Yang^a, Yuchi Lu^d, Tinghan Li^a, Yan Gao^{d,e},
Le Zheng^a, Hang Xiao^f, Tingting Yang^a, Hao Cheng^f, Haibin Huang^f, Yang Liu^f,
Yang Lou^f, Chao Wu^g, Yuxin Chen^{b,g,**}, Haitao Yang^{d,e}, Xiaoyun Ji^{a,g,*},
Hangtian Guo^{a,***}

^a The State Key Laboratory of Pharmaceutical Biotechnology, School of Life Sciences, Nanjing University, Nanjing, Jiangsu, 210023, China

^b Department of Laboratory Medicine, Nanjing Drum Tower Hospital, Nanjing University Medical School, Nanjing, Jiangsu, 210008, China

^c School of Environmental and Biological Engineering, Nanjing University of Science & Technology, Nanjing, Jiangsu, 210094, China

^d Shanghai Institute for Advanced Immunochemical Studies and School of Life Science and Technology, ShanghaiTech University, Shanghai, 201210, China

^e Shanghai Clinical Research and Trial Center, Shanghai, 201210, China

^f Yurogen Biosystem LLC, Wuhan, Hubei, 430075, China

^g Institute of Viruses and Infectious Diseases, Nanjing University, Nanjing, Jiangsu, 210008, China

ARTICLE INFO

Article history:

Received 22 February 2023

Accepted 3 April 2023

Available online 5 April 2023

Keywords:

SARS-CoV-2

Cryo-EM

RmAb

Spike protein

Receptor-binding domain

Antibody development

ABSTRACT

The COVID-19 pandemic, caused by SARS-CoV-2, has led to over 750 million infections and 6.8 million deaths worldwide since late 2019. Due to the continuous evolution of SARS-CoV-2, many significant variants have emerged, creating ongoing challenges to the prevention and treatment of the pandemic. Therefore, the study of antibody responses against SARS-CoV-2 is essential for the development of vaccines and therapeutics. Here we perform single particle cryo-electron microscopy (cryo-EM) structure determination of a rabbit monoclonal antibody (RmAb) 9H1 in complex with the SARS-CoV-2 wild-type (WT) spike trimer. Our structural analysis shows that 9H1 interacts with the receptor-binding motif (RBM) region of the receptor-binding domain (RBD) on the spike protein and by directly competing with angiotensin-converting enzyme 2 (ACE2), it blocks the binding of the virus to the receptor and achieves neutralization. Our findings suggest that utilizing rabbit-derived mAbs provides valuable insights into the molecular interactions between neutralizing antibodies and spike proteins and may also facilitate the development of therapeutic antibodies and expand the antibody library.

© 2023 Elsevier Inc. All rights reserved.

1. Introduction

The Coronavirus disease 2019 (COVID-19) pandemic caused by the β -coronavirus severe acute respiratory syndrome coronavirus 2 (SARS-CoV-2) remains an ongoing global health crisis [1]. SARS-CoV-2 belongs to the coronavirus family, which also includes two previous highly pathogenic coronaviruses severe acute respiratory

syndrome coronavirus (SARS-CoV) and Middle Eastern respiratory syndrome virus (MERS-CoV). The disease was first reported in December 2019 and since early 2020, it has rapidly spread worldwide [2]. As of November 2021, the SARS-CoV-2 variant BA.1 (Omicron, originally found in South Africa) and its sublineages have become the dominant strains circulating globally. This has reversed the trend of previously dominant strains such as B.1.1.7 (Alpha), B.1.351 (Beta), P.1 (Gamma) and B.1.617.2 (Delta) [3–5]. And as of February 17, 2023, more than 756 million people have been infected with COVID-19, resulting in over 6.8 million deaths (<https://covid19.who.int/>).

SARS-CoV-2 is an enveloped, positive-strand RNA virus belonging to the Betacoronavirus genus [6]. Like SARS-CoV, SARS-CoV-2 uses its homotrimeric, glycosylated spike protein to bind the angiotensin-converting enzyme 2 (ACE2) receptor and enter host

* Corresponding author. The State Key Laboratory of Pharmaceutical Biotechnology, School of Life Sciences, Nanjing University, Nanjing, Jiangsu, 210023, China.

** Corresponding author. Department of Laboratory Medicine, Nanjing Drum Tower Hospital, Nanjing University Medical School, Nanjing, Jiangsu, 210008, China.

*** Corresponding author.

E-mail addresses: yuxin.chen@nju.edu.cn (Y. Chen), xiaoyun.ji@nju.edu.cn (X. Ji), guohangtian@nju.edu.cn (H. Guo).

¹ These authors contributed equally: Xiaoyu Chu and Xinyu Ding.

cells [7,8]. The spike protein is formed after its two functional fragments S1 and S2 are proteolytically cleaved by furin-like proteases. The S1 subunit contains an N-terminal domain (NTD, residues 14–305) that recognizes attachment factors and a receptor-binding domain (RBD, residues 328–531) responsible for binding to the host receptor ACE2 [7]. The S2 subunit contains a fusion peptide that facilitates viral and host cell membrane fusion after S1 binds to the receptor. An additional proteolytic cleavage site is located in the S2 region, immediately before the fusion peptide. The RBD undergoes a conformational change between an up (or open) and a down (or closed) conformation, and the binding of RBD to the ACE2 receptor is only possible when it is in the up conformation, as the receptor-binding motif (RBM) is not fully exposed in the down conformation. Due to the immune advantages, the RBD is the most important target recognized by neutralizing antibodies [9]. Therefore, it is essential to develop new therapeutic antibodies that can effectively neutralize SARS-CoV-2 and prepare for potential outbreaks caused by emerging SARS-CoV-2 variants of concern (VOCs) in the future.

Previously, we reported a rabbit monoclonal antibody (RmAb) 9H1 that was able to neutralize the wild-type (WT) SARS-CoV-2 strain in both pseudovirus and authentic virus assays, with IC_{50} values of 14 ng/mL and 26 ng/mL, respectively [10]. In this study, we present the cryo-electron microscopy (cryo-EM) structure of the SARS-CoV-2 WT spike trimer in complex with 9H1 Fabs to provide further insight into the neutralizing mechanisms of 9H1. Our findings show that 9H1 can compete with ACE2 for binding to both the WT and Delta RBD, as demonstrated through competitive ELISA experiments. Moreover, we compare several monoclonal antibodies (mAbs) that share similar epitopes with 9H1 but exhibit broader neutralizing activity to investigate the sensitivity of RBD-targeting antibodies to mutations and provide molecular information for the development of new broad-spectrum antibodies. Our structural data may improve the understanding of interactions between non-humanized antibodies and spike proteins.

2. Materials and methods

2.1. Expression and purification of the SARS-CoV-2 spike protein

Soluble 6P-stabilized SARS-CoV-2 WT and Delta spike proteins were expressed through transient transfection, as previously described [11,12]. In brief, the genes encoding residues 1–1208 of WT and Delta spike ECD were cloned into the pcDNA3.1 mammalian expression vector (Invitrogen) and transfected into FreeStyle 293-F cells (Invitrogen) using polyethyleneimine (PEI, Polysciences). Spike proteins were purified using Ni Sepharose resin (Cytiva) and further purified through gel filtration chromatography using a Superose 6 10/300 column (Cytiva) in $1 \times$ TBS (20 mM Tris-HCl, 200 mM NaCl, pH 8.0).

2.2. Generations of rabbit monoclonal antibody 9H1 against SARS-CoV-2 spike proteins

The generation of RmAb 9H1 involved the use of the SMab platform from Yurogen Biosystems, as previously reported [10]. In brief, rabbits were immunized with DNA vaccines. After single B cell sorting, the successfully recovered IgG variable regions from a positive clone was cloned into a pcDNA3.4 vector for monoclonal antibody expression and purified by protein A affinity chromatography. The resulting RmAbs were then tested for neutralization and ACE2 receptor-blocking abilities.

2.3. Production of 9H1 Fab fragments

RmAbs were buffer exchanged and concentrated to 4 mg/mL before being fragmented using immobilized papain, as previously reported [10]. In brief, the fragmented antibody samples were collected and incubated with immobilized rProtein A Beads 4FF (smart-lifesciences, Cat. No. SA012200), and finally buffer exchanged into $1 \times$ PBS buffer and confirmed using SDS-PAGE.

2.4. Cryo-EM sample preparation and data collection

The SARS-CoV-2 WT spike protein was diluted to 1.0 mg/mL in $1 \times$ PBS and mixed with 9H1 Fab at a 1:3 ratio. To prevent aggregation, 0.01% (w/v) n-dodecyl β -D-maltoside (DDM) was added before the sample was plunge-frozen using a VitroBot IV (ThermoFisher Scientific), with a blot time of 2.5s at -1 force and $8^\circ\text{C}/100\%$ humidity. 4829 micrographs were collected with a defocus range between 1.2 and $2.5 \mu\text{m}$ using a 300 kV Titan Krios microscope (ThermoFisher Scientific) equipped with a K3 detector (Gatan) and SerialEM software [13].

The statistics of cryo-EM data collection can be found in [Supplemental Table 1](#).

2.5. Cryo-EM data processing

The dose-fractionated images were precisely corrected for motion and dose-weighted using MotionCorr2 software [14]. CryoSPARC was used for subsequent steps including CTF estimation, particle picking, extraction, 2D classification, Ab-Initio reconstruction, 3D classification, 3D refinements and local resolution estimation [15]. Non-uniform refinement was used to obtain the final 3D reconstructions, resulting in an overall resolution of 3.25 \AA for the “up/up/up” state (class I) with C3 symmetry, and 3.50 \AA for the “up/up/down” state (class II) with C1 symmetry. A local refinement focused on the WT RBD-9H1 variable domain region was performed to improve the resolution at the binding interface, resulting in a 3.59 \AA map of the RBD-9H1 interface.

The complete cryo-EM data processing workflow is described in [Supplemental Fig. 1](#).

2.6. Model building and refinement

The SARS-CoV-2 WT spike-9H1 Fab complex structures were built by first placing the previous structural model of the WT spike-510A5 Fab complex (PDB: 7WS0) [11] into the cryo-EM electron density maps using UCSF Chimera [16]. The 9H1 Fab model was predicted using Phyre2 [17], then the manual and automated model building were iteratively performed using Coot 0.9.6 [18] and real-space refinement in Phenix 1.20 [19].

The data validation statistics are shown in [Supplemental Table 1](#).

2.7. ELISA experiments

The binding efficacy of 9H1 was assessed using enzyme-linked immunosorbent assay (ELISA) as previously described [10]. In brief, ELISA plates (Corning, Cat. No. 9018) were coated with $25 \mu\text{L}$ of $1 \mu\text{g/mL}$ WT, Delta and Omicron spike ECD or RBD proteins and incubated overnight at 4°C . After washing and blocking, $25 \mu\text{L}$ 9H1 RmAbs of gradient concentrations were added to each well and incubated for 1 h. Then, goat anti-rabbit IgG-HRP was added and incubated for 1 h at room temperature. Thermo TMB substrate was then added and plates were kept in the dark at room temperature. Finally, the OD of 450 nm was measured using the Epoch microplate spectrophotometer (Biotek, USA).

2.8. ACE2 receptor blocking assay

To determine ACE2 competition with 9H1 bound to WT or Delta RBD, a competitive ELISA assay was performed. For WT, biotinylated WT RBD (Kactus Biosystems, CoV-VM4BDB) was coated onto ELISA plates and serially diluted 9H1 was incubated with human ACE2 (Kactus Biosystems, ACE-HM501) before being added to the plates. ACE2 with an hFc tag was detected via goat anti-human IgG-HRP. For Delta, human ACE2 (Kactus Biosystems, ACE-HM501) was coated onto the ELISA plates, and biotinylated Delta RBD (SinoBiological, 40592-V08H91) was incubated with serially diluted 9H1 before being added to the plates, and incubated for 1 h. Biotinylated Delta RBD was detected via neutravidin-HRP. ELISA plates were read at OD 450 nm and 630 nm with an Epoch microplate spectrophotometer (Biotek, USA).

3. Results

3.1. Cryo-EM structure determination of WT spike in complex with 9H1

To understand the structural basis for the binding mode of RmAb 9H1, we determined cryo-EM structures of the prefusion SARS-CoV-2 WT spike trimer in complex with 9H1 Fabs, which are stabilized by six prolines (HexaPro) (Supplemental Fig. 1A and B). Our analysis revealed two distinct classes of WT spike-9H1 Fab complexes, both of which RBD represents a 3-Fab-per-trimer binding mode, with each RBD bound to one 9H1 Fab (Fig. 1A and B). In class I complex, most of the particles are in the “up/up/up” conformation, allowing reconstruction with C3 symmetry to an overall resolution of 3.25 Å (Supplemental Fig. 1C), with all three RBDs tilted at an angle of ~90° (Fig. 3C). In class II complex, most of the particles are in the “up/up/down” conformation, allowing reconstruction with C1 symmetry to an overall resolution of 3.50 Å (Supplemental Fig. 1D). Due to the steric hindrance caused by the binding of 9H1 to the down RBD (RBD_C), one of the up RBD (RBD_B) adopts an unusual over-up conformation with a tilt angle of ~105° (Fig. 3D).

Because of the conformational dynamics of the 9H1-bound RBDs, the electron density in these regions is relatively weak. To further analyze the molecular details of the interaction between 9H1 and RBD, we performed local refinement to improve the resolution of the RBD-9H1 interface to 3.59 Å (Supplemental Fig. 1E). Using the improved density map and a predicted 9H1 Fab structure, we generated structural models that incorporated only the variable heavy chain (VH) and variable light chain (VL) domains of the 9H1 Fab due to the flexible nature of the RBDs (Supplemental Fig. 1F and G).

3.2. Structural basis for the neutralizing mechanism of 9H1

Based on our structural analysis, we then utilized the local-refined model to identify detailed interactions between WT RBD and 9H1 Fab. Like other Class 2 antibodies, 9H1 binds to the RBM region of the RBD regardless of whether it is in the up or down conformation (Fig. 2A) [20]. The complementarity-determining regions (CDRs) of both the light chain (CDRL3) and heavy chain (CDRH3) are located close to the RBM loop (residues 496–506) that connects the β 6 strand and α 5 helix of the RBD, while the CDRL1 mainly interacts with the α 3 helix (residues 403–409) of the RBD (Fig. 2A). Additionally, the CDRH2 contacts the flexible RBM loops (residues 443–447 and 498–502) mainly through hydrophobic interactions (Fig. 2A). The total buried surface area of the WT RBD-9H1 Fab interface is 684 Å² from 9H1 (with 63% of the surface area contributed by the light chain) and 647 Å² from the WT RBD

(Fig. 2B).

At the WT RBD-9H1 interface, RBD residues R403, E406, R408, P499, T500, N501, G502 and Y505 have extensive interactions with the 9H1 VL residues Y29, D30, E90 and S92, and the 9H1 VH residues H55 and Y102 (Fig. 2C). This interaction network is characterized by various hydrogen bonds and salt bridges that are associated with 9H1 CDRs and the RBD amino acid residues located within the 9H1 epitope. Notably, RBD residues T500, N501, G502 and Y505 located on the RBM loop (residues 496–506) are inserted into the cleft between the heavy and light chains of 9H1, where the major hydrogen bond interactions are concentrated.

In our cryo-EM structures, each up or down RBD is decorated with one 9H1 Fab on the RBD, resulting in an epitope that overlaps with the ACE2 binding site. Upon superposition of the up RBDs with the structure of WT RBD-9H1 Fab and RBD-ACE2 complexes, we find significant hindrance between the 9H1 Fab and ACE2 on the same up RBD (Fig. 2D), indicating that 9H1 may compete directly with ACE2 for RBD binding. Our structural analysis was confirmed by competitive ELISA experiments, in which 9H1 was shown to significantly inhibit the binding of ACE2 to both WT RBD and Delta RBD (Fig. 2E). Therefore, 9H1 can block ACE2 binding to the spike trimer, resulting in a neutralizing effect.

3.3. SARS-CoV-2 Omicron variants can escape neutralization by 9H1

Our previous study demonstrated that 9H1 could neutralize not only the SARS-CoV-2 WT strain but also the Delta variant [10,21]. Structural analysis reveals that the Delta RBD has only two mutation sites, L452R and T478K, which are not located on the 9H1 epitope and therefore do not affect the binding of 9H1 to Delta RBD, maintaining its neutralizing activity against the Delta variant. However, the Omicron variant has accumulated a higher number of mutations on its spike protein, including N501Y and Y505H on the BA.1 RBD which severely disrupts the hydrogen bond between RBD and the 9H1 light chain. Other Omicron mutations such as D405 N, V445P, G496S and Q498R, may also affect the RBD-9H1 interactions. Our ELISA experiments have shown that while 9H1 exhibits a high binding capacity to the spike ECD and RBD of both WT and Delta strains, it has lost the ability to bind the BA.1 spike and RBD (Supplemental Fig. 2).

With the emergence of Omicron and its sublineages, the effectiveness of most RBM-targeting neutralizing antibodies, including 9H1, has been significantly affected [22–26]. Interestingly, recent studies have identified new RBM-targeting antibodies with broad-spectrum neutralizing ability against Omicron variants [27–32]. We aim to investigate the mechanisms behind the loss of neutralizing activity of 9H1 against Omicron and the resistance of the other four antibodies to Omicron mutations.

To achieve this, we compared the distribution of epitopes among these antibodies that were highly or partially overlapping with the ACE2 binding site (Fig. 3A). Consistent with our previous description, the 9H1 epitope is mainly located in the RBD₄₉₆₋₅₀₆ loop. This region contains frequent mutations from Omicron BA.1, especially N501Y and Y505H, which disrupt the hydrogen bonds between 9H1 and RBD (Fig. 3B). Additionally, the α 3 helix of RBD (residues 403–409) is another 9H1 epitope region, which also contains mutation sites from BA.2, BA.3 and BA.4/5 (Fig. 3B). Therefore, the interaction between 9H1 and RBD would be severely affected by Omicron mutations, resulting in loss of its neutralizing activity against Omicron variants.

In contrast, F61 [27], GAR05 [28] and S2K146 [29,30] exhibit a larger contact area and more extensive hydrogen bond or salt bridge interactions with the RBD. Besides the RBD₄₉₆₋₅₀₆ loop and RBD₄₀₃₋₄₀₉ helix, these three antibodies also interact with the

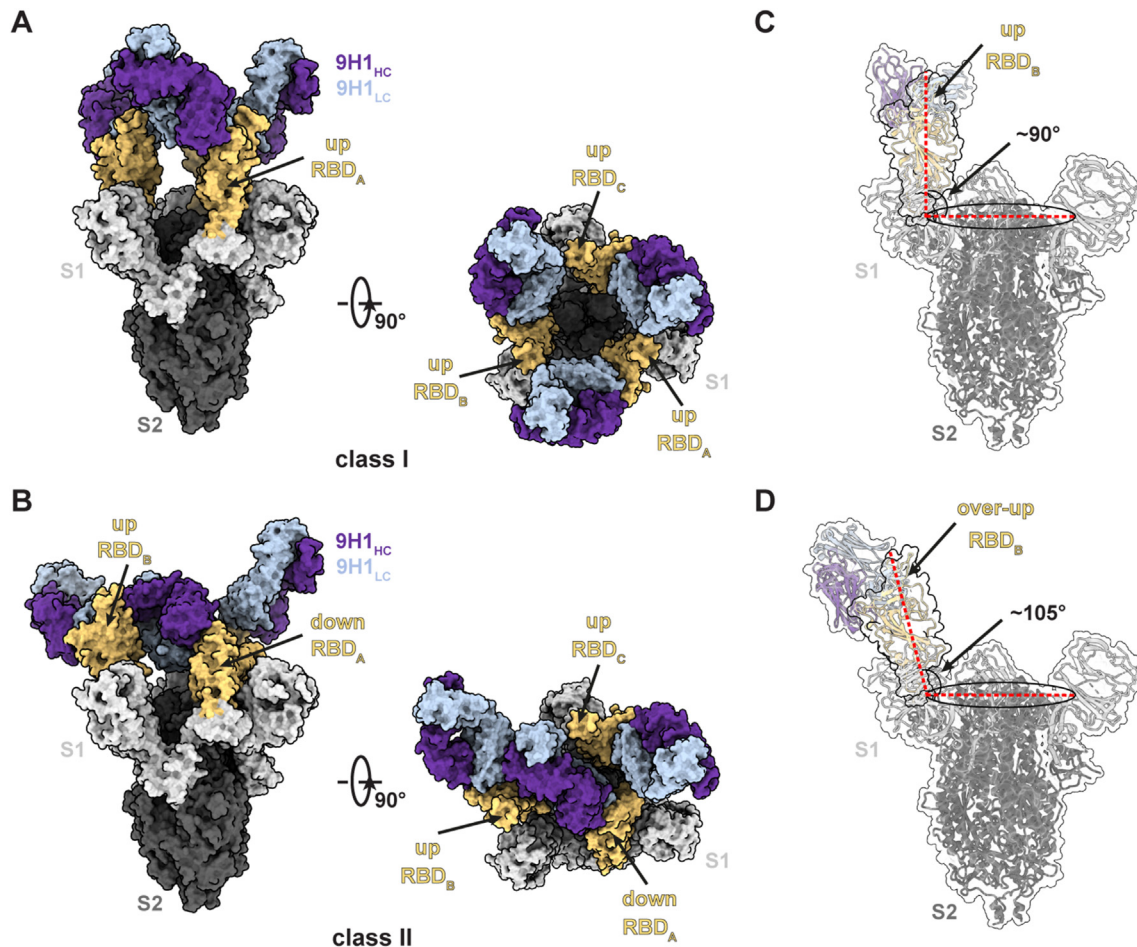


Fig. 1. Cryo-EM structures of WT spike protein in complex with RmAb 9H1. (A and B) The overall cryo-EM structures of the WT spike-9H1 Fab complexes. (A) class I, 3.25 Å, revealing binding of 9H1 to RBDs in the “up/up/up” state; (B) class II, 3.50 Å, revealing binding of 9H1 to RBDs in the “up/up/down” state. (C and D) The tilt angle of the up (C) and over-up (D) WT RBDs are defined by the angle between the long axis of the RBD (red line) and its projection on the horizontal plane (black ellipse). (For interpretation of the references to color in this figure legend, the reader is referred to the Web version of this article.)

RBD₄₈₆₋₄₉₃, RBD₄₅₃₋₄₆₀ and RBD₄₁₅₋₄₂₁ regions. Notably, the epitopes of F61 and GAR05 exhibit significant overlap, while GAR05 has an additional interaction with RBD E484 compared to F61 due to its longer CDRH3 (Fig. 3A and B). In addition, the LY-CoV1404 epitope remains unaffected by the BA.1 mutations, especially N440K, G446S, Q498R and N501Y, suggesting that LY-CoV1404 is not sensitive to these mutations [32]. Hence, despite more than twenty mutation sites being accumulated in the Omicron RBD, the four broad-spectrum mAbs discussed above may form new interactions with some of these mutation sites and maintain robust binding with the RBD. This could explain their potent neutralizing activity against the emerging Omicron variants [27–30,32].

4. Discussion

The emergence of highly mutated SARS-CoV-2 variants, especially the Omicron sublineages, has raised serious concerns about immune evasion, vaccine efficacy, and the need for effective neutralizing antibodies for clinical treatment [22–26]. Although recently reported mAbs have shown broad neutralizing activity against different Omicron sublineages, further research is needed to investigate the binding modes of various antibodies and the molecular mechanisms of interaction between antibodies and the spike protein, which help researchers to develop multifunctional antibodies and expand the therapeutic antibody library. In this

study, we used single-particle cryo-EM to analyze the structure of the prefusion SARS-CoV-2 WT spike trimer in complex with the Fab fragments of RmAb 9H1 to explore its binding mode and neutralizing mechanism. Together with the competitive ELISA experiments, we demonstrate that 9H1 binds to WT RBD and Delta RBD in both up and down conformation and by directly targeting the RBM, 9H1 can compete with ACE2 for RBD binding and thus blocks viral attachment to the receptor and achieves neutralization.

However, the Omicron variant has accumulated a higher number of mutations on its spike protein, which severely disrupt interactions between RBD and the 9H1. In contrast, other RBM-targeting antibodies such as F61, GAR05, S2K146 and LY-CoV1404 have broader neutralizing activity against Omicron variants. These antibodies have a larger contact area and more extensive hydrogen bond or salt bridge interactions with the RBD. Additionally, they may also form new interactions with mutation sites and maintain robust binding with the RBD. These findings can guide the development of new broad-spectrum neutralizing antibodies.

In conclusion, we present high-resolution cryo-EM structures of RmAb 9H1 bound with the SARS-CoV-2 WT spike trimer. The neutralizing potency of rabbit-derived 9H1 highlights the potential of screening neutralizing antibodies from different species. Furthermore, our structural analysis provides valuable insight into the molecular interactions between RmAb and the RBD epitope,

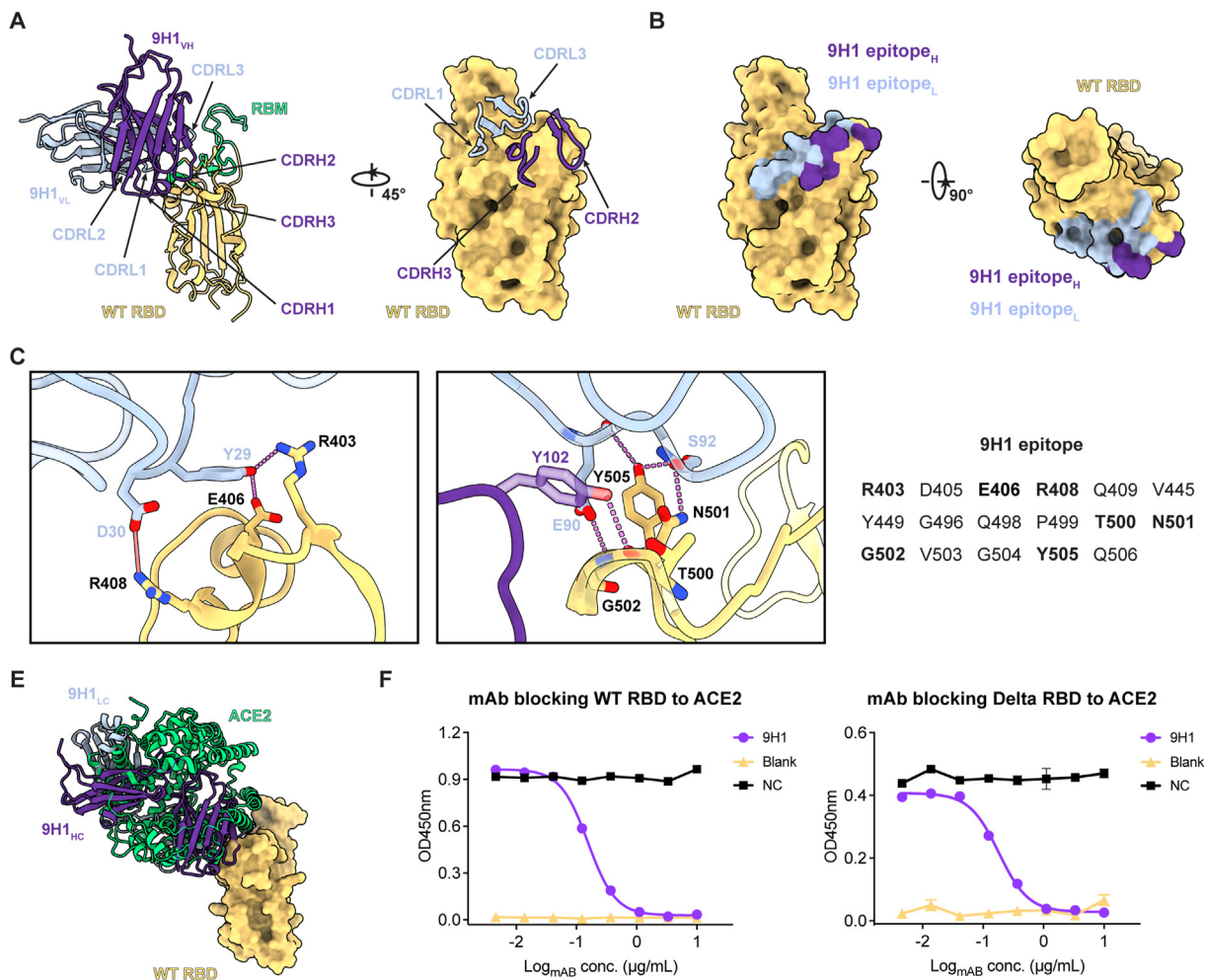


Fig. 2. Structural details of interactions between the WT RBD and 9H1 Fab. (A) The structure model of WT RBD in complex with 9H1 Fab and its CDRs are labeled. The RBM is colored in green. (B) The footprints of the 9H1 heavy chain and light chain are represented as surface and colored purple and steel blue, respectively. (C) Detailed interactions between the WT RBD and 9H1 Fab including 9H1 CDRL1, CDRL3 and CDRH3. The interacting residues of WT RBD are shown as yellow sticks, the 9H1 light chain residues are shown as steel blue sticks and the heavy chain residues are shown as purple sticks. Potential hydrogen bonds are represented as magenta dashed lines and salt bridges are represented by orange lines, respectively. The WT residues recognized by 9H1 are listed. (D) The superposition of the local-refined RBD-ACE2 model (PDB ID: 6M0J) to that of the WT RBD-9H1 Fab model shows significant steric hindrance between 9H1 Fab and ACE2. (E) The ability of 9H1 to compete with ACE2 for binding to WT RBD (left) and Delta RBD (right). The competition capacity of 9H1 was indicated by the level of reduction in the response unit of ACE2 compared with or without the addition of 9H1. (For interpretation of the references to color in this figure legend, the reader is referred to the Web version of this article.)

which can aid in developing new therapeutic antibodies and expanding the antibody library.

Author contributions

H.G., X.J. and Y.C. conceived and designed the project. H.G., X.J. and Y.L. designed the experiments. X.C., Y.Y., T.Y. and L.Z. cloned, expressed and purified spike and RBD proteins. X.D., Y.L., H.H., H.C., Y.L. and Y.Y. were responsible for antibody production and purification and performed ELISA assays for the binding potency of RmAbs. H.G., Y.L. and Y.G. collected and processed cryo-EM data. H.G. built and refined the structure models. X.J., H.Y., H.G., Y.C. and C.W. analyzed and discussed the data. H.G., X.J. and X.C. wrote the manuscript.

Data availability

All data generated and analyzed in this study are provided in the paper and the Supplementary Information. The coordinates and EM map files for the WT spike-9H1 Fab class I complex, WT spike-9H1 Fab class II complex and WT RBD-9H1 Fab local-refined complex have been deposited in the Protein Data Bank (PDB) under accession number 8HEB, 8HEC and 8HED, respectively. For materials requests, please reach out to the corresponding authors.

Declaration of competing interest

The authors declare that they have no known competing financial interests or personal relationships that could have appeared to influence the work reported in this paper.

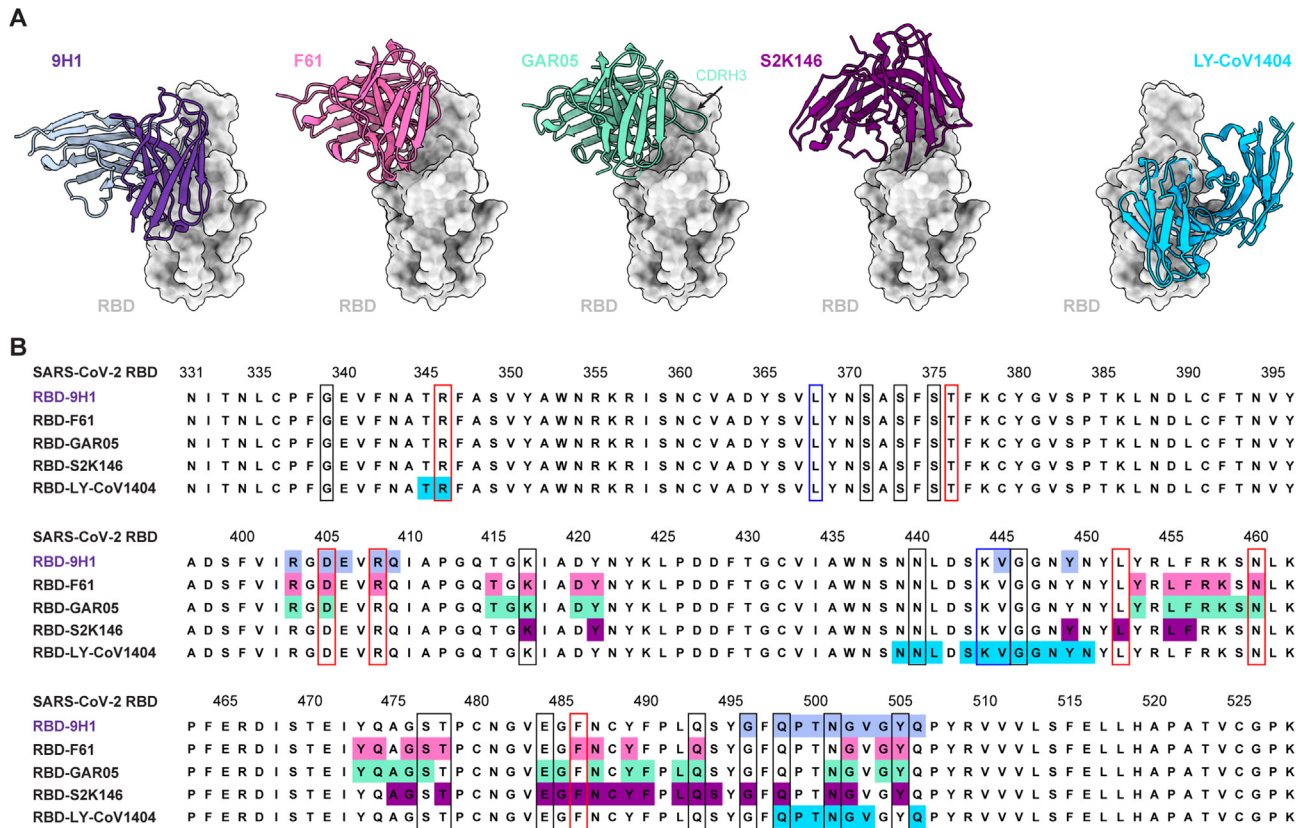


Fig. 3. Comparison of the epitopes of 9H1 and other RBM-targeting mAbs. (A) Structure models of RBD in complex with 9H1 and other four RBM-targeting antibodies that have broad-spectrum neutralizing ability against the Omicron variant. RBD is colored gray. 9H1 Fab is colored consistent with Fig. 1 and the other four Fabs are colored as follows: F61 (PDB ID: 7XMX), hot pink; GAR05 (PDB ID: 7T72), aquamarine; S2K146 (PDB ID 7RAL), dark purple; LY-CoV1404 (PDB ID: 7MMO), sky blue. (B) The sequence of SARS-CoV-2 WT RBD (residues 331–528) with highlighted footprints of mAbs (colored according to the RBD antigenic site recognized). The amino acid substitutions from Omicron BA.1 are marked with black boxes; additional mutation sites from BA.2, BA.3 and BA.4/5 are marked with red boxes; additional mutation sites from BQ.1, BQ.1.1, XBB.1 and XBB.1.5 are marked with blue boxes.

Acknowledgments

We thank the Bio-Electron Microscopy Facility of ShanghaiTech University, and we are grateful to Dr. Qianqian Sun, Dr. Zhihui Zhang and Yaping Wang for their help with cryo-EM technical support.

This work was supported by funds from the National Key Research and Development Program of China (2018YFA0507100, 2016YFD0500300 to X.J.), National Natural Science Foundation of China (grant No. 81871639 to X.J.), Training Program of the Major Research Plan of the National Natural Science Foundation of China, (grant No. 92269118 to Y.C), Scientific Research Project of Jiangsu Health Commission (grant No. M2022013 to Y.C), and the program for Innovative Talents and Entrepreneur in Jiangsu, and the Fundamental Research Funds for the Central Universities.

Appendix A. Supplementary data

Supplementary data to this article can be found online at <https://doi.org/10.1016/j.bbrc.2023.04.002>.

References

[1] N. Zhu, D. Zhang, W. Wang, X. Li, B. Yang, J. Song, et al., A novel coronavirus from patients with pneumonia in China, 2019, *N. Engl. J. Med.* 382 (2020) 727–733, <https://doi.org/10.1056/NEJMoa2001017>.

[2] C. Wang, P.W. Horby, F.G. Hayden, G.F. Gao, A novel coronavirus outbreak of global health concern, *Lancet* 395 (2020) 470–473, [https://doi.org/10.1016/S0140-6736\(20\)30185-9](https://doi.org/10.1016/S0140-6736(20)30185-9).

[3] K. Tao, P.L. Tzou, J. Nouhin, R.K. Gupta, T. de Oliveira, S.L. Kosakovsky Pond, et al., The biological and clinical significance of emerging SARS-CoV-2 variants, *Nat. Rev. Genet.* 22 (2021) 757–773, <https://doi.org/10.1038/s41576-021-00408-x>.

[4] F. Wu, S. Zhao, B. Yu, Y.M. Chen, W. Wang, Z.G. Song, et al., A new coronavirus associated with human respiratory disease in China, *Nature* 579 (2020) 265–269, <https://doi.org/10.1038/s41586-020-2008-3>.

[5] B. Zhou, T.T.N. Thao, D. Hoffmann, A. Taddeo, N. Ebert, F. Labrousseau, et al., SARS-CoV-2 spike D614G change enhances replication and transmission, *Nature* 592 (2021) 122–127, <https://doi.org/10.1038/s41586-021-03361-1>.

[6] X. Xu, P. Chen, J. Wang, J. Feng, H. Zhou, X. Li, et al., Evolution of the novel coronavirus from the ongoing Wuhan outbreak and modeling of its spike protein for risk of human transmission, *Sci. China Life Sci.* 63 (2020) 457–460, <https://doi.org/10.1007/s11427-020-1637-5>.

[7] A.C. Walls, Y.-J. Park, M.A. Tortorici, A. Wall, A.T. McGuire, D. Velesler, Structure, function, and antigenicity of the SARS-CoV-2 spike glycoprotein, *Cell* 181 (2020) 281–292, <https://doi.org/10.1016/j.cell.2020.02.058>.

[8] P. Zhou, X.-L. Yang, X.-G. Wang, B. Hu, L. Zhang, W. Zhang, et al., A pneumonia outbreak associated with a new coronavirus of probable bat origin, *Nature* 579 (2020) 270–273, <https://doi.org/10.1038/s41586-020-2012-7>.

[9] L. Piccoli, Y.J. Park, M.A. Tortorici, N. Czudnochowski, A.C. Walls, M. Beltramello, et al., Mapping neutralizing and immunodominant sites on the SARS-CoV-2 spike receptor-binding domain by structure-guided high-resolution serology, *Cell* 183 (2020) 1024–1042, <https://doi.org/10.1016/j.cell.2020.09.037>.

[10] Y. Chen, L. Zhu, W. Huang, X. Tong, H. Wu, Y. Tao, et al., Potent RBD-specific neutralizing rabbit monoclonal antibodies recognize emerging SARS-CoV-2 variants elicited by DNA prime-protein boost vaccination, *Emerg. Microb. Infect.* 10 (2021) 1390–1403, <https://doi.org/10.1080/22221751.2021.1942227>.

[11] H. Guo, Y. Gao, T. Li, T. Li, Y. Lu, L. Zheng, et al., Structures of Omicron spike complexes and implications for neutralizing antibody development, *Cell Rep.* 39 (2022), 110770, <https://doi.org/10.1016/j.celrep.2022.110770>.

[12] T. Li, X. Han, C. Gu, H. Guo, H. Zhang, Y. Wang, et al., Potent SARS-CoV-2 neutralizing antibodies with protective efficacy against newly emerged mutational variants, *Nat. Commun.* 12 (2021) 6304, <https://doi.org/10.1038/>

- s41467-021-26539-7.
- [13] D.N. Mastronarde, Automated electron microscope tomography using robust prediction of specimen movements, *J. Struct. Biol.* 152 (2005) 36–51, <https://doi.org/10.1016/j.jsb.2005.07.007>.
- [14] S.Q. Zheng, E. Palovcak, J.-P. Armache, K.A. Verba, Y. Cheng, D.A. Agard, MotionCor2: anisotropic correction of beam-induced motion for improved cryo-electron microscopy, *Nat. Methods* 14 (2017) 331–332, <https://doi.org/10.1038/nmeth.4193>.
- [15] A. Punjani, J.L. Rubinstein, D.J. Fleet, M.A. Brubaker, cryoSPARC: algorithms for rapid unsupervised cryo-EM structure determination, *Nat. Methods* 14 (2017) 290–296, <https://doi.org/10.1038/nmeth.4169>.
- [16] E.F. Pettersen, T.D. Goddard, C.C. Huang, G.S. Couch, D.M. Greenblatt, E.C. Meng, et al., UCSF Chimera-A visualization system for exploratory research and analysis, *J. Comput. Chem.* 25 (2004) 1605–1612, <https://doi.org/10.1002/jcc.20084>.
- [17] L.A. Kelley, S. Mezulis, C.M. Yates, M.N. Wass, M.J.E. Sternberg, The Phyre2 web portal for protein modeling, prediction and analysis, *Nat. Protoc.* 10 (2015) 845–858, <https://doi.org/10.1038/nprot.2015.053>.
- [18] P. Emsley, B. Lohkamp, W.G. Scott, K. Cowtan, Features and development of Coot, *Acta Crystallogr. D* 66 (2010) 486–501, <https://doi.org/10.1107/S0907444910007493>.
- [19] D. Liebschner, P.V. Afonine, M.L. Baker, G. Bunkoczi, V.B. Chen, T.I. Croll, et al., Macromolecular structure determination using X-rays, neutrons and electrons: recent developments in Phenix, *Acta Crystallogr. D* 75 (2019) 861–877, <https://doi.org/10.1107/S2059798319011471>.
- [20] C.O. Barnes, C.A. Jette, M.E. Abernathy, K.-M.A. Dam, S.R. Esswein, H.B. Grinstead, et al., SARS-CoV-2 neutralizing antibody structures inform therapeutic strategies, *Nature* 588 (2020) 682–687, <https://doi.org/10.1038/s41586-020-2852-1>.
- [21] H. Guo, Y. Yang, T. Zhao, Y. Lu, Y. Gao, T. Li, et al., Mechanism of a rabbit monoclonal antibody broadly neutralizing SARS-CoV-2 variants, *Commun. Biol.* 6 (2023) 364, <https://doi.org/10.1038/s42003-023-04759-5>.
- [22] Y. Cao, J. Wang, F. Jian, T. Xiao, W. Song, A. Yisimayi, et al., Omicron escapes the majority of existing SARS-CoV-2 neutralizing antibodies, *Nature* 602 (2022) 657–663, <https://doi.org/10.1038/s41586-021-04385-3>.
- [23] Y. Cao, W. Song, L. Wang, P. Liu, C. Yue, F. Jian, et al., Characterization of the Enhanced Infectivity and Antibody Evasion of Omicron BA.2.75, *Cell Host & Microbe*, 2022, <https://doi.org/10.1016/j.chom.2022.09.018>.
- [24] P. Qu, J.P. Evans, Y.-M. Zheng, C. Carlin, L.J. Saif, E.M. Oltz, et al., Evasion of Neutralizing Antibody Responses by the SARS-CoV-2 BA.2.75 Variant, *Cell Host & Microbe*, 2022, <https://doi.org/10.1016/j.chom.2022.09.015>.
- [25] Q. Wang, Y. Guo, S. Iketani, M.S. Nair, Z. Li, H. Mohri, et al., Antibody evasion by SARS-CoV-2 Omicron subvariants BA.2.12.1, BA.4 and BA.5, *Nature* 608 (2022) 603–608, <https://doi.org/10.1038/s41586-022-05053-w>.
- [26] L. Liu, S. Iketani, Y. Guo, J.F.W. Chan, M. Wang, L. Liu, et al., Striking antibody evasion manifested by the Omicron variant of SARS-CoV-2, *Nature* 602 (2022) 676–681, <https://doi.org/10.1038/s41586-021-04388-0>.
- [27] X. Li, Y. Pan, Q. Yin, Z. Wang, S. Shan, L. Zhang, et al., Structural basis of a two-antibody cocktail exhibiting highly potent and broadly neutralizing activities against SARS-CoV-2 variants including diverse Omicron sublineages, *Cell Discovery* 8 (2022) 87, <https://doi.org/10.1038/s41421-022-00449-4>.
- [28] R. Rouet, J.Y. Henry, M.D. Johansen, M. Sobti, H. Balachandran, D.B. Langley, et al., Broadly neutralizing SARS-CoV-2 antibodies through epitope-based selection from convalescent patients, *Nat. Commun.* 14 (2023) 687, <https://doi.org/10.1038/s41467-023-36295-5>.
- [29] E. Cameroni, J.E. Bowen, L.E. Rosen, C. Saliba, S.K. Zepeda, K. Culap, et al., Broadly neutralizing antibodies overcome SARS-CoV-2 Omicron antigenic shift, *Nature* 602 (2022) 664–670, <https://doi.org/10.1038/s41586-021-04386-2>.
- [30] Y.-J. Park, A. De Marco, T.N. Starr, Z. Liu, D. Pinto, A.C. Walls, et al., Antibody-mediated broad sarbecovirus neutralization through ACE2 molecular mimicry, *Science* 375 (2022) 449–454, <https://doi.org/10.1126/science.abm8143>.
- [31] W. Du, D.L. Hurdiss, D. Drabek, A.Z. Mykytyn, F.K. Kaiser, M. González-Hernández, et al., An ACE2-blocking antibody confers broad neutralization and protection against Omicron and other SARS-CoV-2 variants of concern, *Science Immunology* 7 (2022), eabp9312, <https://doi.org/10.1126/sciimmunol.abp9312>.
- [32] K. Westendorf, S. Zentelis, L. Wang, D. Foster, P. Vaillancourt, M. Wiggan, et al., LY-CoV1404 (bebtelovimab) potently neutralizes SARS-CoV-2 variants, *Cell Rep.* 39 (2022), <https://doi.org/10.1016/j.celrep.2022.110812>.